

Table 2.3 (continued)

Page 2

<chem>CaCO3</chem>	Fisher Lot No. 511618, Tested Purity Reagent	
	Alkalies (as SO ₄)	0.002%
	Barium (Ba)	0.000%
	Chloride (Cl)	0.000%
	Heavy Metals	0.000%
	Insol. in HCl and NH ₄ OH ppt.	0.000%
	Iron (Fe)	0.001%
	Mg and Alkali: Salts (as SO ₄)	0.05%
	Sulfate (SO ₄)	0.000%
V	Haynes Metals, 99.888% pure	
Cr	Fisher Lot No. 706302, 99+% Pure Powder	
Mn	Fisher Lot No. 701331, Certified Reagent	
	Assay	99.94%
	Fe	0.003%
Fe	Merck, Reagent Grade, Purified Powder, Reduced by Hydrogen	
Co	Fisher Lot No. 703488, Certified Reagent	
	Assay	99.96%
Ni	Fisher Lot No. 793537, Reduced Powder, Low in CO	
<chem>NiCl2·6H2O</chem>	Mallinckrodt Chem. Works, Analytical Reagent (maximum impurities)	
	Co	0.20%
	Cu	0.002%
	Fe	0.002%
	Pb	0.005%
	Nitrate (NO ₃)	0.01%
	Sulfate (SO ₄)	0.005%
	Insoluble Matter	0.005%
	Subt. not ppt'd by (NH ₄) ₂ S	0.20%
Cu	Fisher Lot No. 792293, Purified Electrolytic Powder	
Cu	Baker Lot No. 6313, Light Turnings	
	Assay (Cu)	100.0%
	Insol. in HNO ₃	0.002%
	Sb and Sn (as Sn)	0.005%
	As	0.0001%
	Fe	0.002%
	Pb	0.001%
	Mn	0.005%
	P	0.0005%
	Ag	0.0005%

Table 2.3 (continued)

Page 3

Zn	Fisher Lot No. 710475, Certified Reagent - Dust	
	Assay	97.0%
	Nitrogen (N)	0.000%
ZnSO ₄ ·7H ₂ O	Fisher Lot No. 761905, Certified A.C.S., Crystal	
	Chloride (Cl)	0.0001%
	Iron (Fe)	0.001%
	Nitrate (NO ₃)	0.002%
	Lead (Pb)	0.001%
	Arsenic (As)	0.0000%
	Insol. Matter	0.001%
	Ammonium (NH ₄)	0.000%
	Manganese (Mn)	0.0002%
	Subt. not ppt'd by (NH ₄) ₂ S as SO ₄	0.09%
As ₂ O ₃	Fisher Lot No. 411685, Tested Purity Reagent	
	Assay	99.8%
	Antimony (Sb)	0.01%
	Chloride (Cl)	0.000%
	Insol. In NH ₄ OH	0.01%
	Lead (Pb)	0.01%
	Non-volatile Matter	0.013%
	Sulfide (S)	0.000%
SeO ₂	MacKay, Certified C.P. Grade	
RbBr	Alfa Inorg. Lot No. 092371	
SrCO ₃	Baker Lot No. 1946, Analyzed Reagent	
	Cl	0.001%
	SO ₄	0.003%
	Insol. in Acetic Acid	0.02%
	Heavy Metals (as Pb)	0.002%
	Ba	0.05%
	Alkali: Salts (as SO ₄)	0.1%
	Fe	0.003%
	NO ₃	0.05%
	Ca	0.3%
Ag	Fisher Lot No. 761789, Certified Reagent, Precipitated Powder	
	Chloride (Cl)	0.005%
	Iron (Fe)	0.0005%
	Copper (Cu)	0.0002%
	Heavy Metals (as Pb)	0.0005%
	Sulfate (SO ₄)	0.0075%

Table 2.3 (continued)

Page 4

AgNO_3	Fisher Lot No. 784877, Certified A.C.S., Crystal	
	Chloride (Cl)	0.0004%
	Iron (Fe)	0.0001%
	Copper (Cu)	0.0006%
	Sulfate (SO_4)	0.001%
	Lead (Pb)	0.0007%
	Subt. not ppt. by HCl	0.007%
Cd	Baker Lot No. 3589, Purified, Mossy	
$\text{Cd}(\text{CH}_3\text{CO}_2)_2 \cdot 2\text{H}_2\text{O}$	Fisher Lot No. 720147, Certified Reagent	
	Insol. Matter	0.003%
	Chloride (Cl)	0.0008%
	Nitrate (NO_3)	0.003%
	Sulfate (SO_4)	0.001%
	Alkalies and Earths	0.03%
	Copper (Cu)	0.0003%
	Iron (Fe)	0.000%
	Lead (Pb)	0.0002%
	Zinc (Zn)	0.02%
$\text{CdCl}_2 \cdot 2\frac{1}{2}\text{H}_2\text{O}$	Fisher Lot No. 750637, Certified Reagent	
	Cu	0.0001%
	Fe	0.0001%
	Zn	0.0%
	Assay (as CdCl_2)	80.5%
	Insol. Matter	0.004%
	NO_3	0.002%
	SO_4	0.002%
	NH_4	0.000%
	Subt. not ppt. by H_2S (SO_4)	0.05%
$\text{CdBr}_2 \cdot 4\text{H}_2\text{O}$	Merck Lot No. 40938, Reagent Grade (maximum impurities)	
	Insol.	0.005%
	Cl	0.2%
	SO_4	0.005%
	Alkalies and Earths	0.20%
	NH_3	0.005%
	Cu	0.002%
	Fe	0.001%
	Pb	0.005%
	Zn	abt 0.03%

Table 2.3 (continued)

Page 5

In	Fisher Lot No. 712132, Certified Reagent	
	Assay	99.99%
Sn	Merck Lot No. 41328, Reagent Grade, Granular (maximum impurities)	20-40 mesh
	As	0.0002%
	Cu	0.002%
	Fe	0.005%
	Pb	0.020%
	Total Foreign Metals	0.05%
Sb	Fisher Lot No. 705470, Certified Reagent, Powder	
	Assay	99.6%
	As	0.00%
	Pb	0.01%
	Fe	0.01%
	Sn	0.0017%
	Cu	0.005%
TeO ₂	Fisher Lot No. 701106, Purified	
BaBr ₂	Amend Drug and Chemical, C.P. Grade	
BaCO ₃	Fisher Lot No. 723948,	
	Oxidizing subt. (as NO ₃)	0.005%
	Chloride (Cl)	0.0005%
	Fe	0.001%
	Insol. Dil. HCl	0.002%
	Subt. not ppt. by H ₂ SO ₄	0.03%
	Heavy Metals (as Pb)	0.0005%
La	British Drug Houses Lot No. 974650, Metal fillings, 99% pure	
CeO ₂	Fisher Lot No. 794342, Purified	
Pr ₆ O ₁₁	Matheson, Coleman & Bell Lot No. PX1635, 99.9%	
Nd ₂ O ₃	Matheson, Coleman & Bell Lot No. NX255, 99.9%	
Sm ₂ O ₃	Alfa Inorg. Lot No. 04039, 99.9%	
Eu ₂ O ₃	Alfa Inorg. Lot No. 061970, 99.99%	
Gd ₂ O ₃	Alfa Inorg. Lot No. 061671, 99.9%	

Table 2.3 (continued)

Page 6

Er_2O_3	Alfa Inorg. Lot No. 03119, 99.9%
Yb_2O_3	Alfa Inorg. Lot No. 01089, 99.9%
Lu_2O_3	MacKay, 99.9%
Pt	Bishop Platinum Works, 3 mil discs
HgBr_2	Alfa Inorg. Lot No. 030571
Pb	Central Scientific, pure foil, silver free
$\text{Pb}(\text{CH}_3\text{CO}_2)_2 \cdot 3\text{H}_2\text{O}$	Fisher Lot No. 793045, Certified A.C.S. Insol. Matter 0.010% Chloride (Cl) 0.0005% Copper (Cu) 0.001% Iron (Fe) 0.0007% Subt. not ppt'd by H_2S (as SO_4) 0.045%
PbBr_2	Fisher Lot No. 770096, Purified
Bi	Baker Lot No. 21836, Analyzed Reagent, Powder Assay (Bi) 100.0% Ag 0.005% Pb 0.0005% As 0.00005% Sb 0.001% Cu 0.0005% Fe 0.002% Zn 0.005%

The table also contains the assays when reported by the manufacturers. With the exception of the Zn metal and the $\text{CdCl}_2 \cdot 2\frac{1}{2}\text{H}_2\text{O}$, all the reagents were assumed to be of 100% purity. Of those specified, the Zn metal was the only reagent with a reported assay of less than 99%. Its certified value of 97% was assumed and used to correct the Zn weight when obtaining the Zn/Cd atom ratio. Since Cd was used as the primary reference element, the purity of the Cd reagents must be well known in order to obtain accurate atom ratios. For this reason, the $\text{CdCl}_2 \cdot 2\frac{1}{2}\text{H}_2\text{O}$ reagent was independently analyzed by two different methods. First, the salt was assayed by determining the chloride content using the Volhard method. The second assay consisted of determining the Cd in the salt by atomic absorption analysis using the method of standard additions. The Cd standard added were prepared from the Cd metal reference reagent. The results from both analyses indicated that the manufacturers reported assay of 80.5% CdCl_2 (see Table 2.3) for the $\text{CdCl}_2 \cdot 2\frac{1}{2}\text{H}_2\text{O}$ reagent was too low by 1.4-1.6%. The agreement between these two measurements implies that the Cd content in the Cd metal reagent is 100%. A more complete description of these analyses is provided in Appendix C.

It must be emphasized that there is an indeterminate uncertainty in the atom ratios because of the assumed purity of the reference reagents. In general, it seems unlikely that this would be greater than 1-2% for any of the reagents.

b) NBS Metal Alloy Standards

Three standard samples of metal alloys were used to test the analytical capability of the method. They are a cast bronze (NBS No. 52),

a tin-base bearing metal (NBS No. 54), and a phosphor bronze bearing metal (NBS No. 63) obtained from the National Bureau of Standards. Their reported assays are provided in Tables 2.4, 2.5 and 2.6. For the filter paper targets, the standards were dissolved in a minimum volume of 6N HCl and diluted with water to about 6 mg/ml (see Table 2.7). NBS No. 63 required a small amount of HNO_3 to be completely taken up into solution. A few drops of HNO_3 were also added to the other two standards to insure dissolution of any small amounts of undissolved solids which may have been present, but were not visible. The standards were dissolved in aqua regia for the lens tissue targets. After taking up in a minimum volume of acid, the solutions were boiled and agitated to expel NO_2 , and diluted to 10-30 mg/ml (see Table 2.7). Lens tissue targets of the standards with a known relative amount of Cd were also prepared by accurately weighing out amounts of the standard and cadmium metal. The samples were dissolved as described above to the concentrations given in Table 2.7. Their known ratios of sample weight to reference Cd weight (m_t/m_{Cd}) are:

NBS-52/Cd	0.5613
NBS-54/Cd	0.9731
NBS-63/Cd	0.6870

c) Others

Two obvious extensions of these targeting procedures are to start directly with liquid samples and to use thin solid samples. For example, the former was used to prepare lens tissue targets of human blood and cows milk. An oak tree leaf served as its own supporting matrix and is an example of the latter case.

Table 2.4

Department of Commerce
Bureau of Standards
Washington

Standard Samples
No. 52

CAST BRONZE

Mix sample well before using

	Percent
Copper	88.33
Tin	7.90
Zinc	1.89
Lead	1.52
Antimony	0.16
Nickel	0.13
Iron	0.12

Table 2.5

Department of Commerce
Bureau of Standards
Washington

Standard Samples
No. 54

TIN-BASE BEARING METAL

Mix sample well before using

	Percent
Tin	88.24
Antimony	7.33
Copper	3.75
Lead	0.56
Iron	0.06
Bismuth	0.05
Arsenic	0.05

Table 2.6

Department of Commerce
Bureau of Standards
Washington

Standard Samples
No. 63

PHOSPHOR BRONZE BEARING METAL

Mix sample well before using

	Percent
Copper	78.05
Tin	9.91
Lead	9.74
Phosphorous62
Antimony55
Zinc48
Iron27
Arsenic19
Sulphur06
Aluminum05
Nickel008

Table 2.7

Sample Solutions for Target Preparation of NBS Standards

Filter Paper Targets

NBS-52	5.68 mg/ml
NBS-54	5.77 mg/ml
NBS-63	6.45 mg/ml

Lens Tissue Targets

NBS-52	16.6 mg/ml
NBS-54	32.6 mg/ml
NBS-63	9.87 mg/ml

NBS-52/Cd	20.5 mg/ml + 36.6 mg/ml Cd
NBS-54/Cd	60.0 mg/ml + 62.5 mg/ml Cd
NBS-63/Cd	22.3 mg/ml + 32.5 mg/ml Cd

2.2.3 Target Composition and Evaluation of Solution Sampling Technique

The procedure used to prepare the targets assumes that the atom ratios in the targets is identical to that in their sample solutions. Since this assumption is of paramount importance to the procedure, it was decided to check this assumption for a number of cases by independent chemical analyses of the solutions and targets. An exhaustive study of the Cu/Cd and Pb/Cd lens tissue targets over a wide variation of sample solution concentrations and atom ratios was made.

In the case of the starting sample solutions, analyses were made on aliquot portions of the same solution used to prepare the targets. The targets were analyzed by taking a known area of the target, digesting it in concentrated nitric acid, and extracting a known aliquot part of the liquid. The determinations for Cu, Cd and Pb were made by atomic absorption analysis using the standard additions method and the procedures prescribed by Perkin-Elmer (PE68) for their Model 303 spectrophotometer. The light sources were hollow cathode lamps employing the 3247 Å Cu line, the 2288 Å Cd line, and the 2833 Å Pb line for the Cu, Cd and Pb analyses, respectively. All three procedures used an air-acetylene flame to atomize the samples. Both sets of unknown liquid samples (starting solutions and respective targets) were diluted and adjusted to about 2.5 µg/ml Cu for the Cu analyses, to about 1.0 µg/ml Cd for Cd analyses, and to about 10.0 µg/ml Pb for the Pb analyses. For each analysis, three solutions were prepared, as follows, for the absorption measurements: a) the unknown to the adjusted concentration, b) the unknown to the adjusted concentration plus a known standard addition at a concentration of about one-half times the adjusted

amount, c) the unknown to the adjusted concentration plus a known standard addition at a concentration of about one times the adjusted amount. The unknown solution concentrations were determined from the known standard additions by a best linear fit to the three measured absorbance values.

The results of the thirteen cases studied are provided in Table 2.8 for the Cu/Cd targets and Table 2.9 for the Pb/Cd targets. For the Cu/Cd targets studied, the starting solutions ranged from 0.5 to 0.1 M Cd with $a_{\text{Cu}}/a_{\text{Cd}}$ atom ratios of 1.0, 0.1 and 0.01; whereas, the starting solutions for the Pb/Cd targets ranged from 0.25 to 0.05 M Cd with $a_{\text{Pb}}/a_{\text{Cd}}$ atom ratios of 2.0 and 0.2. For each target, the tables contain the molarity and atom ratio of the starting solution which was calculated from the known sample weights of the starting reagents, the target thickness in mg/cm^2 which was obtained from direct weighing of the target, the thickness (mg/cm^2) of each element in the target and its weight percentage of the total target weight as determined by the atomic absorption analyses, and the measured atom ratios in the solutions and in the targets. As indicated, in the tables, there is a good correspondence between the atom ratio measured in the solutions and that of the target. Furthermore, both measurements are in good agreement with the known atom ratios obtained from the sample weights. The several percent differences in the measurements are random in that they do not reflect any systematic trends, and they indicate the measurement precision. Therefore, it appears that the solution sampling technique used for the target preparation is well founded.

Table 2.8
Composition of Cu/Cd Lens Tissue Targets

<u>Σ Cd</u>	<u>$(a_{Cu}/a_{Cd})^*$</u>	<u>Target Thickness⁺ (mg/cm²)</u>	<u>Cu in Target **</u>		<u>$(a_{Cu}/a_{Cd})^{**}$</u>		<u>% Difference⁺⁺</u>
			<u>mg/cm²</u>	<u>%, by weight</u>	<u>mg/cm²</u>	<u>%, by weight</u>	
0.5	0.9335	0.952	0.140	14.7	0.263	27.6	0.942
0.25	0.9335	0.502	0.0730	14.5	0.144	28.7	0.897
0.1	0.9335	0.220	0.0295	13.4	0.0555	25.0	0.940
0.5	0.09791	0.677	0.0165	2.44	0.303	44.8	0.0980
0.25	0.09791	0.312	0.00745	2.39	0.138	44.2	0.0947
0.1	0.09791	0.123	0.00290	2.36	0.0525	42.7	0.0964
0.5	0.01381	0.627	0.00207	0.330	0.258	41.1	0.0133
0.25	0.01381	0.293	0.000970	0.331	0.133	45.4	0.0137
0.1	0.01381	0.127	0.000436	0.343	0.0565	44.5	0.0128

*Obtained from known sample weights.

+Obtained from direct weighing, excludes paper thickness (1.355 mg/cm²).

**Measured by atomic absorption analysis.

$$++ \frac{(a_{Cu}/a_{Cd})_{target} - (a_{Cu}/a_{Cd})_{solution}}{(a_{Cu}/a_{Cd})_{solution}} \times 100$$

Table 2.9
Composition of Pb/Cd Lens Tissue Targets

Starting Pb/Cd Solution Used to Prepare Target	Target Thickness ⁺ (mg/cm ²)	Pb in Target*		Cd in Target**		$(\alpha_{Pb}/\alpha_{Cd})^{**}$	% Difference ⁺⁺
		mg/cm ²	% by weight	mg/cm ²	% by weight		
0.5	0.25	2.0050	1.220	0.508	41.6	0.136	11.1
0.1	0.05	2.0050	0.285	0.116	40.7	0.0314	11.0
0.05	0.25	0.1968	0.532	0.0666	12.5	0.187	35.2
0.01	0.05	0.1968	0.172	0.0214	12.4	0.0593	34.5
						0.197	0.196
						2.018	2.026
						1.984	2.004
						0.195	0.193
						0.197	0.196
						+ 0.4	+ 0.4
						+ 1.0	+ 1.0
						- 1.0	- 1.0
						+ 0.5	+ 0.5

*Obtained from known sample weights.

⁺Obtained from direct weighing, excludes paper thickness (1.355 mg/cm²).

^{**}Measured by atomic absorption analysis.

$$++ \frac{(\alpha_{Pb}/\alpha_{Cd})_{target} - (\alpha_{Pb}/\alpha_{Cd})_{solution}}{(\alpha_{Pb}/\alpha_{Cd})_{solution}} \times 100$$

The amount of sample material on a target appears to governed by the Freundlich empirical isotherm for adsorption from solution:

$$\frac{m_x}{m_a} = k C_x^n$$

where m_x is the mass of material x adsorbed onto mass m_a of adsorbent, C_x is the concentration of x in solution when equilibrium is reached, and k and n are empirical constants [cf. Moore (M62), p. 749]. The data for Cu in the Cu/Cd targets (Table 2.8) and for Pb in the Pb/Cd targets (Table 2.9) is well represented by this empirical relation. It also applies, but to a lesser extent, for the Cd in both the Cu/Cd and Pb/Cd targets. By fitting the data* to the Freundlich equation, the constant n for the three cases was found to be

$$n(\text{Cu}) = 0.93 \pm 0.03$$

$$n(\text{Pb}) = 0.86 \pm 0.06$$

$$n(\text{Cd}) = 0.86 \pm 0.11$$

Therefore, if the constant k does not vary drastically from case to case, the two predominate factors determining the total amount of sample material on the target are the starting solution concentration, C_x , and the mass, m_a , of the adsorbent supporting matrix for the target. The net effect of this is that the target weights should be approximately similar for all the targets prepared from solutions with the same starting solution concentration. This, in fact, was evidenced as indicated by the data of Table 2.10 where the sample thicknesses for a wide range

*The precision of the data and the variance of the fit did not warrant obtaining the constant k .

Table 2.10
Sample Thickness for Lens Tissue Targets

Target	Target Sample Thickness* (mg/cm ²)	Target	Target Sample Thickness* (mg/cm ²)
Ca/Cd	0.770	Ba/Cd	0.881
V/Cd	0.490 ⁺	La/Cd	0.276 ⁺
Cr/Cd	1.147	Nd/Cd (2)	0.787
Mn/Cd	0.679	Gd/Cd (1)	1.151
Fe/Cd	1.029	Gd/Cd (2)	1.029
Co/Cd	0.926	Er/Cd	1.202
Ni/Cd	0.812	Yb/Cd	1.157
Zn/Cd	1.178	Pt/Cd	0.805 ⁺
Se/Cd	0.644	Hg/Br/Cd	0.420
Br/Cd	0.880	Pb/Cd	1.027
In/Cd	0.719	Bi/Cd	0.927
Sn/Cd	1.190	V/Zn	0.288 ⁺
Te/Cd	0.973	Cr/Ni	0.164 ⁺

*Does not include the 1.355 mg/cm² thickness of lens tissue supporting matrix.

⁺Prepared from < 0.5 M solutions.

of targets prepared from ~ 0.5 M solutions are given. As indicated, the targets of the very heavy elements [e.g., Pb/Cd (1.03 mg/cm^2) or Bi/Cd (0.93 mg/cm^2)] are not necessarily heavier than those of the medium [e.g., Sn/Cd (1.19 mg/cm^2) or In/Cd (0.72 mg/cm^2)] or the light [e.g., Mn/Cd (0.68 mg/cm^2) or Fe/Cd (1.03 mg/cm^2)] elements. The thicknesses of the targets listed in Table 2.10 are only meant to be representative. Since it was not necessary, no attempt was made to establish controls for duplicating the sample thicknesses of targets prepared from the same starting solutions. For this reason, a wide variation in thicknesses for a given target can be expected. Furthermore, it is not unreasonable to suspect that there may be some cases which deviate drastically from the Freundlich equation, or specific cases where the empirical constants k and n may be markedly different from those of the other cases.

The lens tissue targets which have a sample thickness of approximately 1 mg/cm^2 contain about 10^{18} atoms/ cm^2 of each element. This is the order of magnitude range for all the reference and NBS sample targets. The thickness of the sample material on the filter paper targets is typically 2-3 times that of the lens tissue targets for the same starting solution concentration. Therefore, the thickness of 1.35 mg/cm^2 for lens tissue compared to 8.15 mg/cm^2 for the filter paper presents a more favorable sample to backing mass ratio in the former case.

2.3 X-Ray Spectrometers and Detection Configurations

The non-dispersive X-ray spectrometers used to detect and measure X-rays from the target employed liquid nitrogen cooled lithium-drifted silicon or germanium semiconductor detectors. The Si(Li) detector (Princeton Gamma-Tech LS23) had a 4 mm diameter x 3 mm deep sensitive (active) region with a 7 mm diameter x 0.025 mm thick Be entrance window. The manufacturer specifications for its resolution was 216 eV at 6.4 keV.* The Ge(Li) detector (Ortec GX-299B) had a 6 mm diameter x 4.79 mm deep sensitive region. Its absorbing dead layers were a 0.13 mm thick Be window and $40.4 \mu\text{g/cm}^2$ gold. The resolution (manufacturer specifications) was 177 eV at 5.9 keV and 494 eV at 122 keV.[†] Both detectors were coupled to charge sensitive FET preamplifiers [Princeton Gamma-Tech RS-10 for Si(Li), and Ortec 118A for Ge(Li)]. Pulses from the preamplifiers were amplified (Ortec 452 Spectroscopy Amplifier) and analyzed with a 4096-channel 50 MHz ADC (Northern Scientific NS-625) interfaced to a PDP-15 on-line computer. The amplifier output presented unipolar pulses with a 1 μsec shaping time constant and 93 Ω impedance to the ADC. A lower level discriminator on the ADC was used to cut out electronic noise and to keep the deadtime less than several percent. Provision was available to gate the ADC from a scaler (Ortec 430) driven by a current integrator (Brookhaven Instruments Corp., Model 1000) which monitored the electron beam. The on-line computer

*This resolution was obtained at a count rate of 10^3 cps with a 9.3 μsec shaping time constant.

[†]Resolution obtained with 5 μsec shaping time constant on ORTEC 400 amplifier.

served as both the memory device for the spectrometer and for simple data reduction. The pulse-height analysis routine was written by B. E. Chi of the SUNY/Albany, Physics Department.

These two spectrometers were employed in four different systems (i.e., the combination of the detector and geometry) for the measurements. In each system, the detector was located at 90° with respect to the incident electron beam direction. In Systems A and B, the Si(Li) detector observed the target through a Mylar window on the target chamber. The Ge(Li) detector was used in a similar manner for System C. In System D, the Si(Li) was vacuum coupled to the target chamber and observed the target directly.

2.3.1 Systems A and B: Si(Li)

In System A, the target chamber (4" beam tube cross) was fitted with a 2.54 cm diameter x 0.051 mm thick Mylar window. This X-ray exit window was mounted with a vacuum seal to a brass blank-off on the chamber and was located at 10.2 cm from the target centre. The 0.025 mm thick Be entrance window on the Si(Li) detector was located at 90° to the incident electron direction at a distance of 17.1 cm from the Mylar exit window. Thus, an X-ray originating at the target centre evidenced a 27.3 cm path in going to the detector. This path consisted of 10.2 cm vacuum, 0.051 mm Mylar, 17.1 cm air and 0.025 mm Be.

The incident X-ray direction to the detector was shielded with a 2.54 cm diameter graded collimator of 5.1 cm lead, 2.5 cm iron and 0.65 cm aluminum. An attempt was made to further collimate the X-rays with a 6 mm diameter hole in a 5 cm thick plastic plug. This

was not used since alignment of the electron beam and detector axes became too critical. The Si(Li) detector was recessed 6.1 cm behind the graded collimator and was shielded on the sides with 1.6 mm copper and 4.0 mm brass. The entire setup, including the detector cryostat, was further protected from background radiation, mainly from the beam dump, by lead and concrete shielding. A minimum of 5 to 15 cm of lead was used to shield the sides, including bottom and top, of the detector. The cryostat was primarily shielded with concrete.

System B was almost identical to that of System A except that a 1000 gauss sweeping magnet was interposed between the iron and aluminum in the graded collimator. The magnet was used to sweep scattered electrons away from the front of the entrance window and prevent them from entering the detector. This was extremely beneficial in reducing the background in the X-ray spectra. Figure 2.8 contains a schematic of the arrangement for System B. System A is similar to this general layout except the sweeping magnet was not present. For comparison, the distance from the Mylar window to the Si(Li) detector was 17.1 cm in System A and 22.0 cm in System B.

2.3.2 System C: Ge(Li)

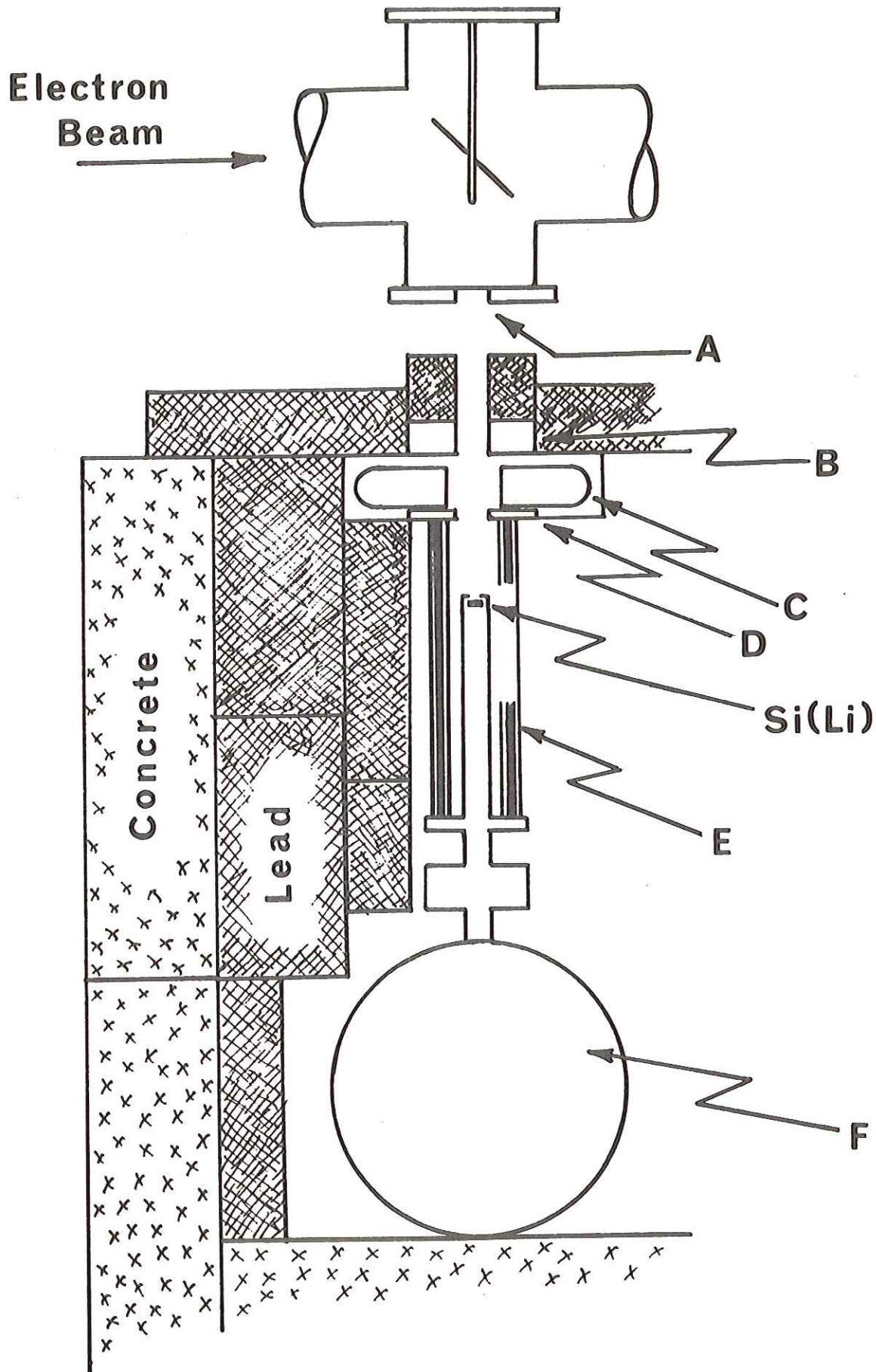
In this system, a Ge(Li) detector was located at a distance of 38.6 cm from the Mylar exit window on the target chamber and at 90° to the incident electron beam direction. With this configuration, the path for an X-ray from the centre of the target to the detector consisted of 10.2 cm vacuum, 0.051 mm Mylar, 38.6 cm air, and 0.13 mm Be. The path was collimated with the same collimator, lead (5.1 cm) - iron (2.5 cm) -

FIGURE 2.8
Physical Arrangement for System B

The lead and concrete shielding to the right of the detector and cryostat is not shown.

Legend

- A: Mylar exit window
- B: iron collimator
- C: sweeping magnet
- D: aluminum collimator
- E: copper and brass shield
- F: detector liquid nitrogen cryostat



aluminum (0.65 cm), described in Section 2.3.1. The 1000 gauss sweeping magnet was molded into a 5.1 x 15.2 x 20.3 cm plastic cast with a 4 cm hole between the pole pieces. The cast was made with a commercial liquid casting plastic.* The purpose of the plastic cast was to present the swept electrons with a low Z material, instead of allowing them to interact with higher Z metals of the magnet which would produce a higher bremsstrahlung and X-ray background. The magnet in the plastic cast was located between the iron and aluminum in the collimator. The sides of the detector were shielded with a 0.65 cm thick aluminum cylindrical shield. A schematic of this arrangement is shown in Figure 2.9. All sides of the detector was further shielded with a minimum of 5 cm lead. To prevent background radiation from entering from the rear of the assembly, the entire cryostat was shielded with 10 cm thick concrete.

2.3.3 System D: Si(Li) - Vacuum Coupled

For System D, the Si(Li) detector was directly vacuum coupled to the target chamber. The detector was located at a distance of 51.5 cm from the target centre at 90° to the electron beam. The only absorbing layer in the X-ray path was the 0.025 mm Be entrance window on the detector. The detector was connected to the target chamber through a vacuum gate valve. The gate valve was used to keep the region in front of the entrance window evacuated during target changing. The connecting link between the gate valve and the detector consisted of a 4" to 2" beam tube reducer, a 2" bellows and a 3.5 cm diameter copper tube. A

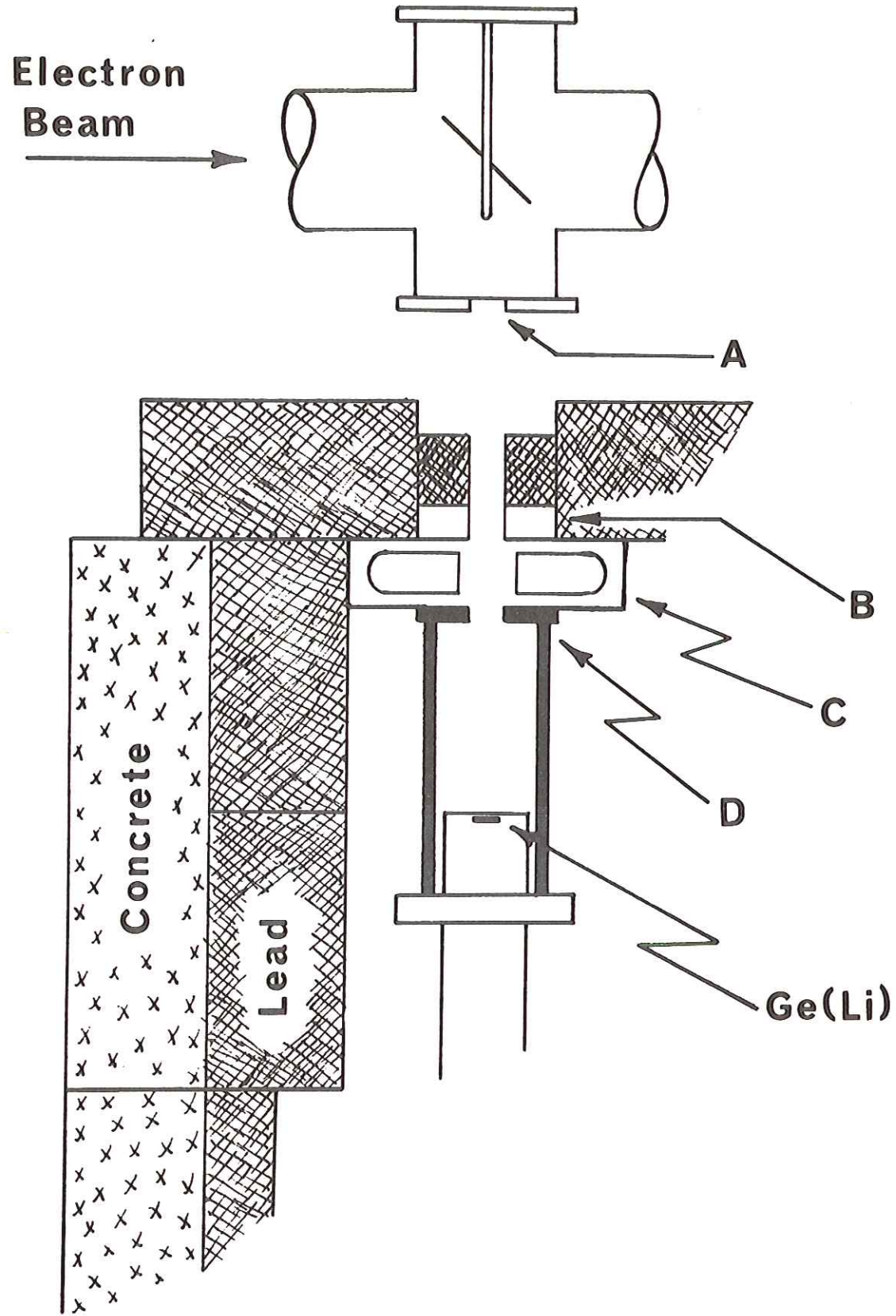
*Clear Cast, a product of American Handicrafts Company, Forth Worth, Texas.

FIGURE 2.9
Physical Arrangement for System C

The lead and concrete shielding to the right of the detector is not shown. The liquid nitrogen cryostat (not shown) was shielded with concrete.

Legend

- A: Mylar exit window
- B: iron collimator
- C: sweeping magnet in plastic cast
- D: aluminum collimator and shield



3.2 cm diameter cylindrical aluminum tube extended 20 cm in front of the detector and served as a collimator and shield. It was fitted between the detector snout and the copper connecting tube. The direction in front of the detector was provided with a 2.5 cm thick iron collimator and shield and with the sweeping magnet in the plastic cast. The sides of the detector was shielded with the copper and aluminum tubes described above and with the copper and brass cylindrical shield described in Section 2.3.1. The physical arrangement for this system is shown in Figure 2.10. As in the prior systems, the entire setup including cryostat was further shielded from background radiation with lead and concrete.

2.4 Measurement Procedures and Data Analysis

A general outline of the procedure for a given run used to obtain an X-ray spectrum from a target follows:

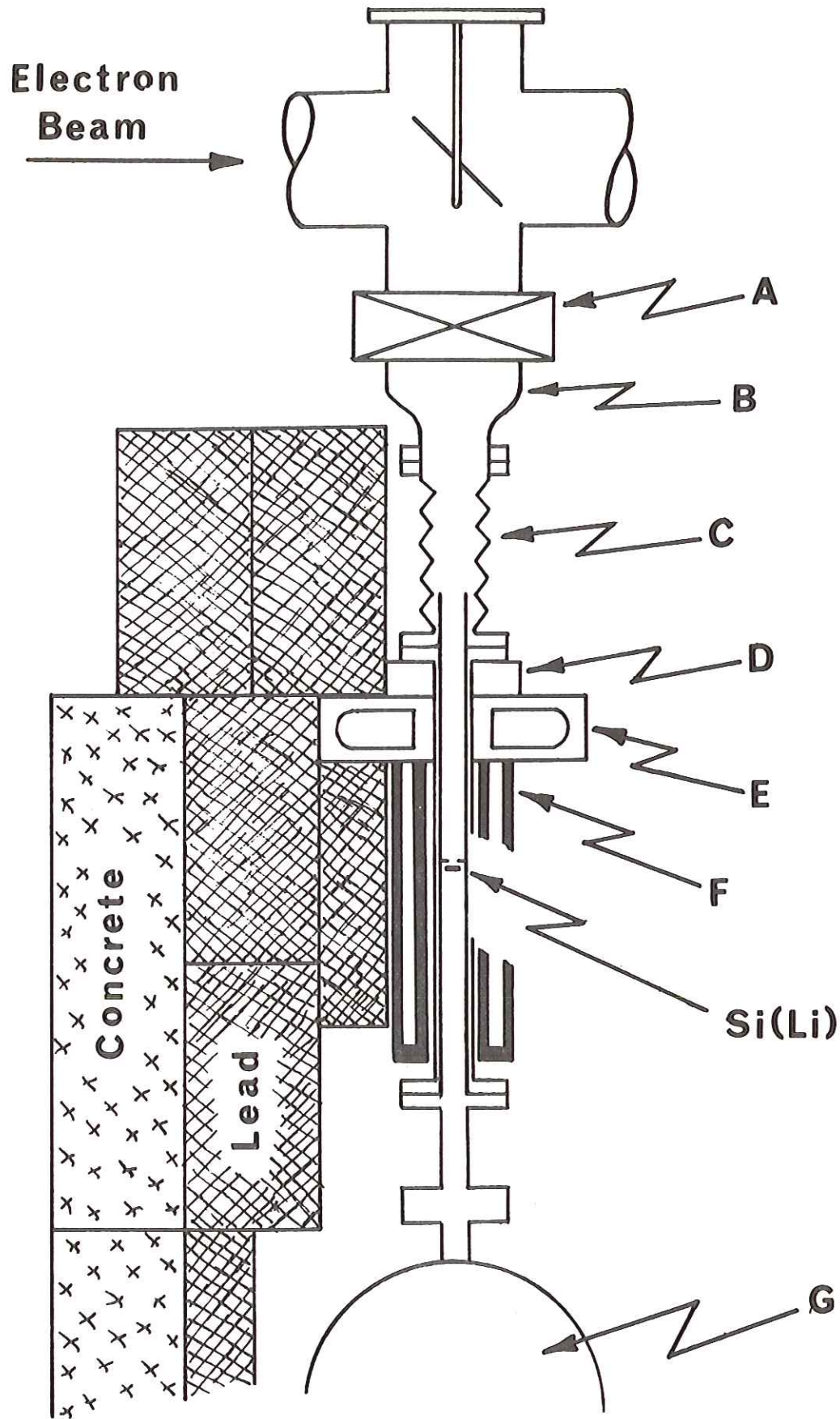
- i) Close off the accelerator vacuum. (For System D, first close the detector gate valve.)
- ii) Open the experimental section to air and mount the target in the target chamber.
- iii) Close the target chamber and evacuate the experimental section.
- iv) Open the experimental section to the accelerator vacuum. (For System D, first open the detector gate valve).
- v) Irradiate the target with accelerated electrons at a given energy and average beam current.
- vi) Accumulate the X-ray spectrum from the target with the given spectrometer.

FIGURE 2.10
Physical Arrangement for System D

The lead and concrete shielding to the right of the detector is not shown. The liquid nitrogen cryostat (not shown) was also shielded with lead and concrete.

Legend

- A: vacuum gate valve
- B: beam tube reducer
- C: bellows
- D: iron collimator
- E: sweeping magnet in plastic cast
- F: copper and brass shield



Obviously, this procedure must be preceded by calibrating and positioning the electron beam (Section 2.1), by preparing the target (Section 2.2), and by setting up the X-ray spectrometer (Section 2.3). During each run, the electron beam was monitored by current measurements. Since various sections of the experimental beam line were electrically isolated (see Figure 2.4), considerable flexibility in monitoring was possible. Several of these possibilities are to monitor the current 1) on the entire experimental section ($C_1 + C_2 + C_3 + C_4 + C_5$), 2) only that entering the beam dump ($C_3 + C_4 + C_5$), or 3) just that on the target chamber. The effect of the target on the electron beam could also be monitored. For example, an estimate of the extent of electron backscatter from the target could be made by measuring the ratio of the current on C_1 to that on ($C_2 + C_3 + C_4$), or the degree of electron scattering could be estimated from simultaneous monitoring of the various sections. Accumulation of the spectrum for a given run could be terminated after a given charge collection (integrated electron current), after a given analysis livetime, or simply after sufficient counting statistics are generated. In most of the runs, the spectra were obtained for an integral amount of charge collection (e.g., 200 microCoulomb). The analysis livetime for the run was also recorded. Although these two parameters were not necessary for any of the measurements, they were useful in making a rapid comparison of different runs to ascertain whether the experimental conditions had changed.

The resultant spectrum obtained from a run contains the K and L X-rays of all the elements present in the target. There is a limit of detectability for the lowest energy X-rays however, because of

self-absorption and absorption by materials interposed between the sample and the detector. The lowest energy detectable X-ray depends on the specific detection system used. The functional dependence of the peak shapes in the spectra is extremely complex since most of the X-ray peaks are unresolved multiplets of closely lying X-ray lines. They were not resolved because of the finite detection resolution of the spectrometers which was typically 250-400 eV (FWHM). For this reason, it is an inherently difficult task to adopt a general algorithm for an accurate integrating procedure which is valid for all peaks in a spectrum. Since an accurate determination of the "true" number of X-rays in a peak was not of primary importance to this work, it was decided to use a consistent procedure which was easily reproducible. The selected procedure which is based on a numerical integration over the peak area follows. Neglecting the tails, the rising and falling edges of a peak are approximately linear on a logarithmic scale*. The interval between the intercepts of these linear edges and the background was considered to be the "peak width". The foreground was obtained by summing the data in the channels over this peak width. The shape of the background under the peak was estimated by drawing a smooth curve between the data in channels on each side of the peak. The background was then obtained by taking the area (number of counts) under this fitted curve over the peak width. The uncertainty in the measurement of the number of X-rays in the peak is

$$\sigma_N = \sqrt{\sigma_F^2 + \sigma_B^2 + (\Delta c_B)^2} , \quad (2.1)$$

*This is due to the nearly Gaussian or Lorentzian shape of the peaks which has been experimentally demonstrated by many works [cf. Varnell and Trischuk (VT69) and references therein].

where σ_F and σ_B are the standard deviations for the statistical fluctuations in the measurements and are approximated by the square root of the number of counts in the foreground and background, respectively. The term ΔC_B represents the additional uncertainty in locating the "true" background and is taken as the difference between the area for a maximum and minimum fitted curve. The procedure described above was used throughout this work and by necessity underestimates the "true" number of X-rays. Since all of the measurements were relative however, and the integrating procedure was standardized, the results are internally consistent. Most of the peaks observed were not singlets, but rather were multiplets of closely lying X-ray lines. Those multiplets which were not resolved were treated as single peaks. Doublets which were partially resolved were stripped into two single peaks using the same peak shape criteria (linear rising and falling edges on logarithmic scale) and fitted to the doublet shape. Higher order multiplets were not stripped. The uncertainty in the number of X-rays must include the additional uncertainty in selecting the "true" peak admixture. This additional term is taken as the difference between an estimated maximum and minimum admixture and must be included in the radical of Equation 2.1. Peak stripping of unresolved and partially resolved X-rays from two or more different elements is described in the following sections.

2.4.1 Relative X-Ray Yields

The reference samples, containing a known amount of primary reference element and at least one other element, were used to establish the relative X-ray yields. The yields reflect not only the X-ray

production (ionization cross section and fluorescence yield) but also the efficiency of observation for a particular target and detector configuration, and it includes the effects of geometry and absorption. Cadmium was used as the primary reference element with the Cd K α X-ray yield taken as unity. This definition was purely arbitrary since any other element or any other X-ray yield could have been chosen as the standard. In each spectrum obtained from electron irradiation of the reference targets, the number of X-rays in each X-ray line was measured relative to the yield of the Cd K α X-ray yield. That is, the relative yield for the η X-ray of element Z is

$$Y_{\eta}(Z) = \frac{N_{\eta}(Z)}{N_{K\alpha}(Cd)} \left(\frac{a_{Cd}}{a_Z} \right) \quad (2.2)$$

where $N_{\eta}(Z)$ is the measured number of η X-rays from element Z, $N_{K\alpha}(Cd)$ is the measured number of Cd K α X-rays, and (a_Z/a_{Cd}) is the known atom ratio of element Z to Cd. These yields refer not only to a particular element Z, but also to a particular X-ray line η . The yields for each distinguishable K or L X-ray peak could be measured, e.g. for the K α , K β , L α_1 or L β lines. A knowledge of the ratio of these yields for a given element is useful in the spectral analysis. For example, although the Sn K α and the Cd K β X-rays are not completely resolved, a prior knowledge of the Cd K β /K α yield ratio permits a stripping out of the Sn K α yield. This allows essentially an unequivocal analysis of a pair of nearby elements provided that at least one of the major X-ray lines can be resolved.

The relative yields can also be measured with respect to a secondary reference element once its relative yield with respect to the Cd K α yield is established. The relative yield for element Z' measured with respect to a secondary reference element Z is

$$Y_{Z'} = Y_Z \frac{N_{Z'}}{N_Z} \left(\frac{a_Z}{a_{Z'}} \right) \quad (2.3)$$

where Y_Z is the previously determined relative yield for Z (Equation 2.2), $N_{Z'}$ and N_Z are the respective measured number of X-rays from elements Z' and Z, and $(a_{Z'}/a_Z)$ is the known Z' to Z atom ratio in the target. The effect of Equation 2.3 is that although the yield $Y_{Z'}$ is measured relative to a secondary reference element Z, it is still expressed on a basis relative to the Cd K α yield. The important consequence of this is that the yields of all the elements can be determined relative to each other.

2.4.2 Elemental Analysis

A detection system is essentially calibrated for quantitative elemental analysis once the relative yields are measured. This method is well suited for the simultaneous assay for many constituent elements in an unknown since its X-ray spectrum contains the detectable K and L X-rays for all the elements present in the sample. Relative amounts of each constituent element are determined from the measured X-ray intensities in the spectrum and their relative yields. To illustrate, the weight fraction of element A with respect to element B in an unknown sample is

$$\frac{m_A}{m_B} = \frac{N_\mu(A)}{N_\nu(B)} \frac{W_A}{W_B} \frac{Y_\nu(B)}{Y_\mu(A)}, \quad (2.4)$$

where $[N_\mu(A)/N_\nu(B)]$ is the ratio of the measured number of μ X-rays from element A to the number of ν X-rays from element B obtained from the same spectrum, and where $Y_\mu(A)$ and $Y_\nu(B)$ refer to the respective relative yields [Equation 2.2] for μ X-ray of element A and ν X-ray of element B. The atomic weight ratio, W_A/W_B , is used to convert the relative yields from an atom to mass basis.

Not all the elements in a sample are necessarily observed due to detection limitations. Therefore, the single measurement described above will not account for the total amount of sample unless all of the constituent elements are detected. With unknown samples, this condition is never known with certainty, and an additional measurement is necessary to obtain the true percentage of the element in the unknown. This second measurement is made with a known relative amount of an internal reference element added to the sample. For a sample containing a known ratio, (m_{total}/m_Z) , of unknown sample weight, m_{total} , to reference element Z weight, m_Z , the weight fraction of element A in the unknown, (m_A/m_{total}) is obtained from:

$$\frac{m_A}{m_{\text{total}}} = \frac{N_\mu(A)}{N_\eta(Z)} \frac{W_A}{W_Z} \frac{Y_\eta(Z)}{Y_\mu(A)} \frac{m_Z}{m_{\text{total}}} , \quad (2.5)$$

where $[N_\mu(A)/N_\eta(Z)]$ is the ratio of the measured number of μ X-rays for element A to the η X-rays for reference element Z, and where $Y_\eta(Z)$, $Y_\mu(A)$ and W_A/W_Z are given as before. For these studies, Cd was also used as the internal reference element.

The assay of an element can be made by analysis of any one of several of its X-rays provided the relative yield for this X-ray has been previously measured. This offers considerable flexibility in

making the analyses. For example, the unfavorable detection efficiency for the K X-rays of high Z elements can be circumvented by analyzing its L X-rays for the determination. In the case that all of an element's X-ray peaks are masked by other elements X-rays, the intensity for one of its X-rays can normally be obtained by utilizing known yield ratios (e.g., $K\beta/K\alpha$) and by stripping. The masked line can be stripped by a numerical curve fitting procedure using standard line shapes obtained from the reference sample spectra for the single peaks. The procedure used is similar to that described by Birks (B69). Specific examples using this stripping procedure are described in Section 3.1 of the Results.

The entire procedure for measuring the relative yields and making elemental assays, outlined in Equation 2.2 through 2.5, requires only relative measurements. All of the measured quantities are obtained from ratios of simultaneously recorded X-ray intensities and weight ratios. It, therefore, does not require any absolute measurements of the number of atoms in the targets or the number of X-rays produced.

Part 3

RESULTS AND DISCUSSION

3.1 Relative X-Ray Yields and Elemental Analysis

All of the electron irradiations for these studies were made at a calibrated (see Section 2.1.1) electron beam energy of 2.04 ± 0.01 MeV. Typically, the runs were of 5-60 minute duration with electron currents of 10-100 nA. The major experimental differences in the four series of measurements (Systems A, B, C and D) follows:

- System A filter paper targets and the Si(Li) detector without the sweep magnet (see Section 2.3.1).
- System B filter paper targets and the Si(Li) detector (see Section 2.3.1).
- System C lens tissue targets and the Ge(Li) detector (see Section 2.3.2).
- System D lens tissue targets and the Si(Li) detector vacuum coupled to the target chamber (see Section 2.3.3).

The spectra obtained with System A had a higher background than those from the other three systems. This higher background was due to low energy electrons getting into the detector. These electrons arose from scattering of the primary beam by the target and secondary electrons (delta rays) from ionization of the target and surrounding materials. The sweep magnet used in the other three systems magnetically deflected the electrons from the detector entrance windows and thereby prevented them from entering the detectors. Furthermore, the spectra obtained with filter paper targets (Systems A and B) had a higher background than the spectra obtained with lens tissue target (Systems C and D). This was to be expected because of the more favorable sample

material to paper backing mass ratio with the latter. It was found that the majority of background radiation in any of the spectra originated at the target. This was discovered by moving the targets downstream in the target chamber out of the line of sight of the detectors. In this way, the detectors could not directly observe the radiation from the target while the electron beam was still scattered by the target to the same extent. Various attempts at further shielding (see Section 2.3) of the beam dump produced no noticeable changes in the background of the spectra. This also demonstrated the fact that the majority of the spectral background originated from bremsstrahlung produced in the target. For this reason, thin targets with the most favorable sample material to supporting matrix mass ratio are most useful.

The procedure used to determine the relative yields from the various reference targets was described in Section 2.4. The results for the relative $K\alpha$ and $K\beta$ X-ray yields, $Y_{K\alpha}(Z)$ and $Y_{K\beta}(Z)$, measured with Systems B, C and D are presented in Tables 3.1, 3.2 and 3.3, respectively. These measurements are also graphically displayed in Figure 3.1. The most striking feature of these yields is that their values are comparable over a wide range of elements. For example, with the Ge(Li) detector in System C, the $K\alpha$ X-ray yields vary by less than a factor of 7 from bromine ($Z = 35$) to bismuth ($Z = 83$). Similarly, the $K\alpha$ X-ray yields obtained with the Si(Li) detector in System D change by only a factor of 10 from vanadium ($Z = 23$) to barium ($Z = 56$). Thus, the sensitivity for quantitative determination over the entire range of elements from $Z = 23$ to $Z = 83$ is rather comparable.

Table 3.1
Relative K X-Ray Yields for System B
[normalized to $Y_{K\alpha}(Cd) = 1$]

Element	Z	$Y_{K\alpha}(Z)$	$Y_{K\beta}(Z)$	$Y_{K\alpha}(Br)*$	$Y_{K\beta}(Br)$	$Y_{K\beta}(Cd)*$
Mn	25	1.530	0.303	-	-	0.175
Fe	26	1.890	0.353	-	-	0.172
Ni	28	1.789	0.263	2.637	0.458	0.170
Cu	29	2.734	0.411	-	-	0.176
Zn	30	3.005	0.466	-	-	0.171
Rb	37	2.451	0.394	(2.816)	0.471	-
Sn	50	0.747	0.130	-	-	(0.172)
Ba	56	0.334	0.0578	(2.816)	0.466	-
Nd	60	0.129	0.0245	2.736	0.450	0.166
Gd	64	0.0854	0.0136	2.930	0.485	0.181
Er	68	0.0497	0.0102	3.006	0.494	0.172
Lu	70	0.0343	0.00680	2.769	0.464	0.174
Pb	82	0.0128	0.00188	-	-	0.166

*Values in parentheses were assumed for the spectrum analysis.

Table 3.2
Relative K X-Ray Yields for System C
[normalized to $Y_{K\alpha}(Cd) = 1$]

Element	Z	$Y_{K\alpha}(Z)$	$Y_{K\beta}(Z)$	$Y_{K\beta}(Cd)*$
Br	35	1.309	0.260	0.226
Ag	47	1.193	0.249	(0.224)
In	49	0.968	0.202	(0.224)
Sn	50	0.972	0.214	(0.224)
Sb	51	0.960	0.214	(0.224)
Te	52	0.870	0.199	(0.224)
Ba	56	0.734	0.185	0.225
Nd	60	0.541	0.136	0.228
Sm	62	0.534	0.135	0.223
Gd	64	0.524	0.135	0.229
Er	68	0.451	0.111	0.222
Yb	70	0.409	0.0973	0.219
Pt	78	0.284	0.0678	0.222
Pb	82	0.223	0.0480	0.219
Bi	83	0.209	0.0432	0.229

*Values in parentheses were assumed for the spectrum analysis.

Table 3.3
Relative K X-Ray Yields for System D
[normalized to $Y_{K\alpha}(\text{Cd}) = 1$]

Element	Z	$Y_{K\alpha}(Z)$	$Y_{K\beta}(Z)$	$Y_{K\beta}(\text{Cd})^*$
Al	13	0.471	-	-
S	16	1.312	-	-
Cl	17	1.896	-	-
K	19	2.597	-	-
Ca	20	2.908	-	-
V	23	3.197	0.400	0.170
Cr	24	2.821	0.376	0.170
Mn	25	3.196	0.431	0.174
Fe	26	3.403	0.457	0.173
Co	27	3.593	0.522	0.171
Ni	28	3.876	0.553	0.177
Cu	29	3.583	0.512	0.171
Zn	30	3.618	0.523	0.167
As	33	3.209	0.485	0.174
Se	34	2.818	0.434	0.176
Br	35	3.105	0.494	0.173
Rb	37	2.901	0.471	0.170
Sr	38	2.583	0.433	0.173
Ag	47	1.348	0.226	(0.172)
In	49	0.881	0.138	(0.172)
Sn	50	0.815	0.127	(0.172)
Sb	51	0.704	0.116	(0.172)
Te	52	0.610	0.0967	(0.172)
Ba	56	0.331	0.0579	0.167
La	57	0.192	0.0343	0.172
Ce	58	0.214	0.0369	0.172

Table 3.3 (Continued)

Relative K X-Ray Yields for System D

[normalized to $Y_{K\alpha}(Cd) = 1$]

Element	Z	$Y_{K\alpha}(Z)$	$Y_{K\beta}(Z)$	$Y_{K\beta}(Cd)*$
Pr	59	0.198	0.0366	0.170
Nd	60	0.156	0.0219	0.168
		0.157	0.0277	0.170
Sm	62	0.127	0.0222	0.165
Eu	63	0.118	0.0219	0.173
Gd	64	0.106	0.0175	0.169
		0.107	0.0178	0.168
Er	68	0.0589	-	0.158
Yb	70	0.0431	-	0.162

*Values in parentheses were assumed for the spectrum analysis.

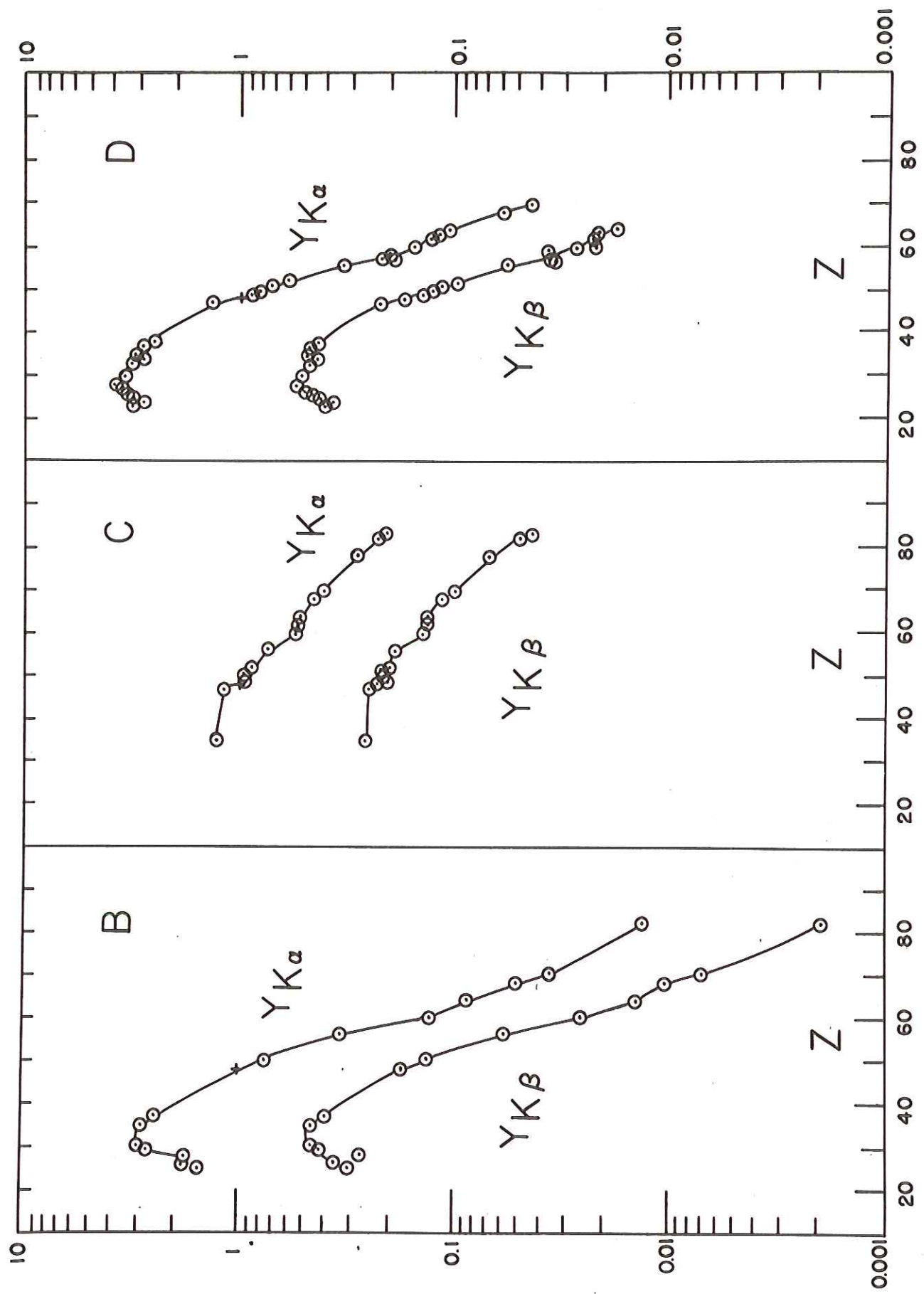
FIGURE 3.1

Relative K X-Ray Yields ($Y_{K\alpha}$ and $Y_{K\beta}$) as a Function
of Atomic Number (Z) for Systems B, C and D

System B: Si(Li)

System C: Ge(Li)

System D: Si(Li)-Vacuum Coupled



The differences in the relative yields for a given element as measured with the various systems are essentially due to the differences in the target transmission, the attenuation by materials interposed between the target and detector, and the intrinsic detection efficiency for the detector. For low energy X-rays, the vacuum path and thin entrance window (0.025 mm Be) associated with the Si(Li) detector in System D was definitely favored over the air path and thicker windows (0.13 mm Be and 0.051 mm Mylar) used with the Ge(Li) detector in System C. Similarly, the thicker filter paper targets and air path used with the Si(Li) detector in System B was not as advantageous for low energy X-rays as the lens tissue targets and vacuum path used with the same detector in System D. These differences in target transmission and attenuation are clearly evident in the relative yields for the light element X-rays. For example, the relative yield for the Mn K α X-ray in System B is reduced by over a factor of two in comparison to that measured with System D (compare Table 3.1 and 3.3).

At high X-ray energies, where absorption and attenuation are no longer dominant factors, the Ge(Li) detector is more advantageous since it has a much larger intrinsic detection efficiency than the Si(Li) detector [cf. Israel, et. al. (ILS71) and Campbell, et. al (CM72)]. This higher efficiency for the Ge(Li) detector is apparent if one compares the shape of the relative yield curves as shown in Figure 3.1 for Systems B and D (Si(Li) detector) to that for System C (Ge(Li) detector). Both the Ge(Li) and Si(Li) detector are nearly 100% efficient below 10 keV. The efficiency of the Si(Li) detector begins to decrease at \sim 15 keV and falls off rapidly above 20 keV such that at 50 keV, it is only

~ 15% efficient and less than 2% efficient at 100 keV. On the other hand, the Ge(Li) intrinsic efficiency never goes below 80% for X-ray energies up to 100 keV. There is a sharp drop in the efficiency at the Ge K-edge (11.1 keV) where it reaches its minimum (~ 80%), but gradually increases again to nearly 100% at 50 keV. In the region above 50 keV it decreases slowly to about 90% at 100 keV.

Although the Ge(Li) detector is more efficient at high energies, it exhibits large escape peak losses [cf. Israel, et. al. (ILS71) and Palms, et. al. (PRW68)], which makes its use rather disadvantageous for analysis of unknown samples. The disadvantage is not just the depletion of the photopeak intensity, but even more the fact that a complicated set of escape peaks occur in the spectra. This effect is illustrated in Figure 3.3b for the Ag/Cd reference target where several of these escape peaks are shown. They result from escape of both the Ge K α and Ge K β X-rays for each of the four major lines from Ag and Cd. Thus, for even this simple case with only two elements present in the sample, eight escape peaks can arise which correspond to:

$$\text{Cd K}\alpha - \text{Ge K}\alpha = 23.1 - 9.9 = 13.2 \text{ keV}$$

$$\text{Cd K}\alpha - \text{Ge K}\beta = 23.1 - 11.0 = 12.1 \text{ keV}$$

$$\text{Cd K}\beta - \text{Ge K}\alpha = 26.2 - 9.9 = 16.3 \text{ keV}$$

$$\text{Cd K}\beta - \text{Ge K}\beta = 26.2 - 11.0 = 15.2 \text{ keV}$$

$$\text{Ag K}\alpha - \text{Ge K}\alpha = 22.1 - 9.9 = 12.2 \text{ keV}$$

$$\text{Ag K}\alpha - \text{Ge K}\beta = 22.1 - 11.0 = 11.1 \text{ keV}$$

$$\text{Ag K}\beta - \text{Ge K}\alpha = 25.0 - 9.9 = 15.1 \text{ keV}$$

$$\text{Ag K}\beta - \text{Ge K}\beta = 25.0 - 11.0 = 14.0 \text{ keV}$$

The relative sizes of the escape peaks are primarily dependent on the relative intensities of the X-ray transitions, $K\beta/K\alpha$ [i.e., the transition probability ratios (NSS70)], and on the ratio of the escape peak to photopeak intensity, R. For example, the relative intensities of the escape peaks due to incident Ag K α X-rays with $R(\text{AgK}\alpha) = 0.045$ (PRW68) are

$$I(\text{Ag K}\alpha) = 1$$

$$I(\text{Ag K}\alpha - \text{Ge K}\alpha) = \frac{R(\text{Ag K}\alpha)}{1 + R(\text{Ag K}\alpha)} \left[1 + \frac{K\beta}{K\alpha} (\text{Ge}) \right] = 0.038$$

$$I(\text{Ag K}\alpha - \text{Ge K}\beta) = \frac{R(\text{Ag K}\alpha)}{1 + R(\text{Ag K}\alpha)} \frac{K\beta}{K\alpha} (\text{Ge}) \left[1 + \frac{K\beta}{K\alpha} (\text{Ge}) \right] = 0.0054$$

where the transition probability ratio for Ge, $\frac{K\beta}{K\alpha}(\text{Ge})$, is 0.142 (NSS70).

Similarly, since the $K\beta/K\alpha$ ratio for Ag is 0.212 (NSS70), the relative intensities for the Ag K β X-ray and its corresponding escape peaks are

$$I(\text{Ag K}\beta) = \frac{K\beta}{K\alpha} (\text{Ag}) = 0.212$$

$$I(\text{Ag K}\beta - \text{Ge K}\alpha) = \frac{R(\text{Ag K}\beta)}{1 + R(\text{Ag K}\beta)} \frac{K\beta}{K\alpha} (\text{Ag}) \left[1 + \frac{K\beta}{K\alpha} (\text{Ge}) \right] = 0.0097$$

$$I(\text{Ag K}\beta - \text{Ge K}\beta) = \frac{R(\text{Ag K}\beta)}{1 + R(\text{Ag K}\beta)} \frac{K\beta}{K\alpha} (\text{Ag}) \frac{K\beta}{K\alpha} (\text{Ge}) \left[1 + \frac{K\beta}{K\alpha} (\text{Ge}) \right] = 0.0014$$

where the Ag K β escape peak loss correction, $R(\text{Ag K}\beta)$, is 0.055 (PRW68).

A similar set of relative escape peak intensities can be obtained for the incident Cd X-rays using the same procedure. Obviously the relative sizes of the escape peaks due to two different elements are dependent on the relative intensities of the incident X-rays from these elements.

The presence of these escape peaks affects the spectral analysis in two ways. First, the escape peaks resulting from one element can underlie the photopeaks of another element. An example of

this is shown in Figure 3.3a for the Br/Cd reference sample where the (Cd K α - Ge K α) and (Cd K β - Ge K β) escape peaks are completely masked by the intense Br K α and K β photopeaks. In this situation, the escape peak loss corrections, R, for Cd must be measured and their values known before one can obtain accurate Br photopeak intensities. The second effect, which can be more serious, is that an escape peak may be mis-identified as the photopeak of some another element. Although, this can usually be avoided by a careful examination of the spectrum it is not an unlikely mistake for the novice who is unfamiliar with escape peak phenomena.

The Si(Li) detector also exhibits escape peak losses (see, for example, Figure 3.2a and Appendix A). However, the loss is very small in comparison to that for the Ge(Li) detector. This is a result of the low fluorescent yield of 0.047 for Si compared to the value 0.540 for Ge (BCF72). At the K-edge, where the escape peak losses are largest, the correction R for the Si(Li) detector is less than 0.02 while R for the Ge(Li) detector is nearly 0.20 (ILS71). For both detectors, R decreases rapidly above their K-edges, but the large initial value and higher K-edge for Ge makes the losses significant up to 50 keV where R = 0.01 for the Ge(Li) detector. In comparison, the value of R \approx 0.01 is reached at 3 keV for the Si(Li) detector (ILS71).

The efficiency disadvantage of the Si(Li) detector at high energies can be circumvented by analysis of the heavy elements via their L X-ray lines. If one uses the K X-rays for elements up to Z \sim 60 and the L X-ray lines for elements above this, the Si(Li) is almost as

FIGURE 3.2

Typical X-Ray Spectra of the Reference Samples
Obtained with the Si(Li) Detector (System D)

- (a) Cu/Cd (atom ratio: 1.0458) after 40 minute run with 2 MeV electrons at 20 nA current.
- (b) Sn/Cd (atom ratio: 0.7761) after 14 minute run with 2 MeV electrons at 50 nA current.
- (c) Pb/Cd (atom ratio: 2.0278) after 27 minute run with 2 MeV electrons at 50 nA current.

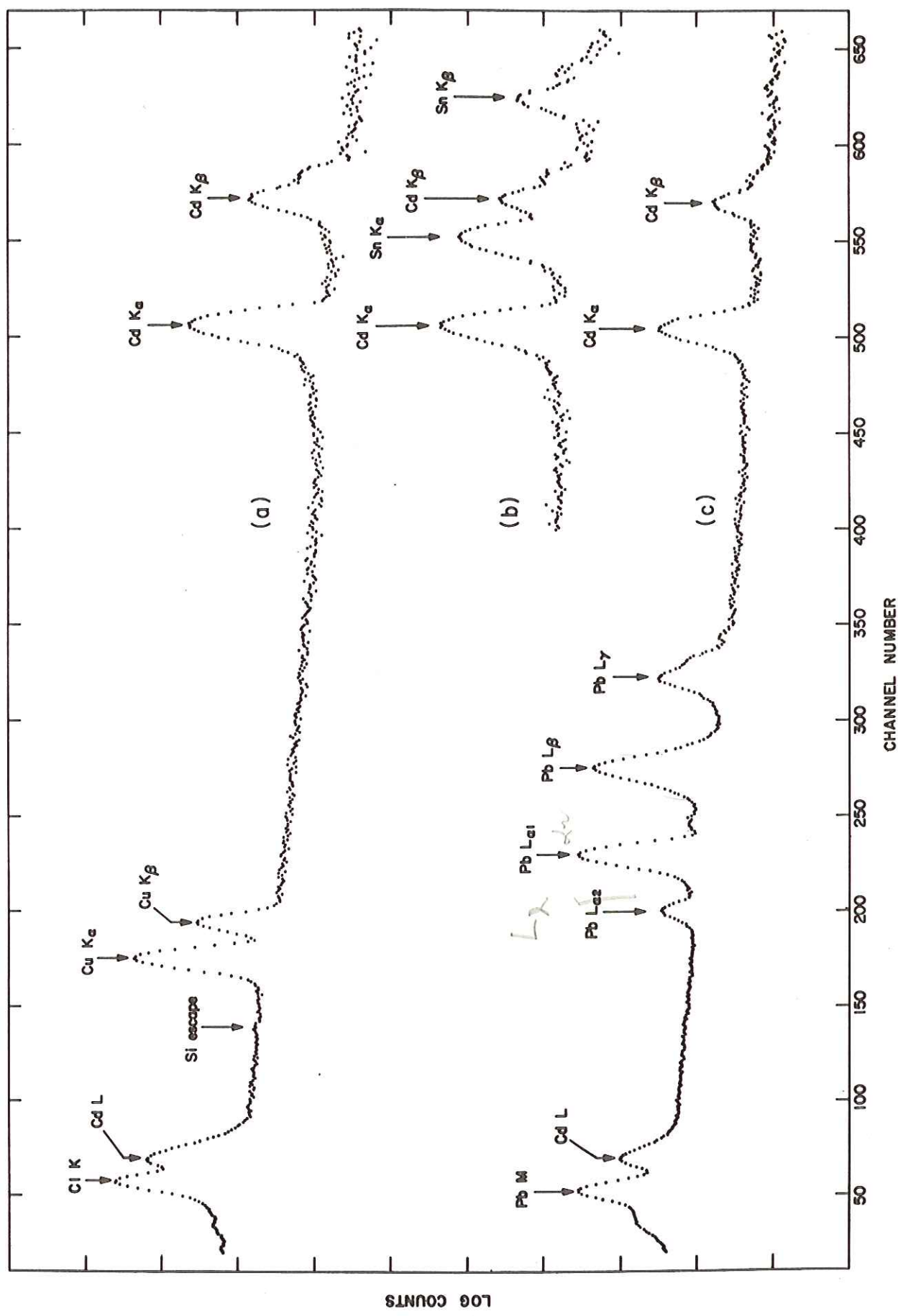
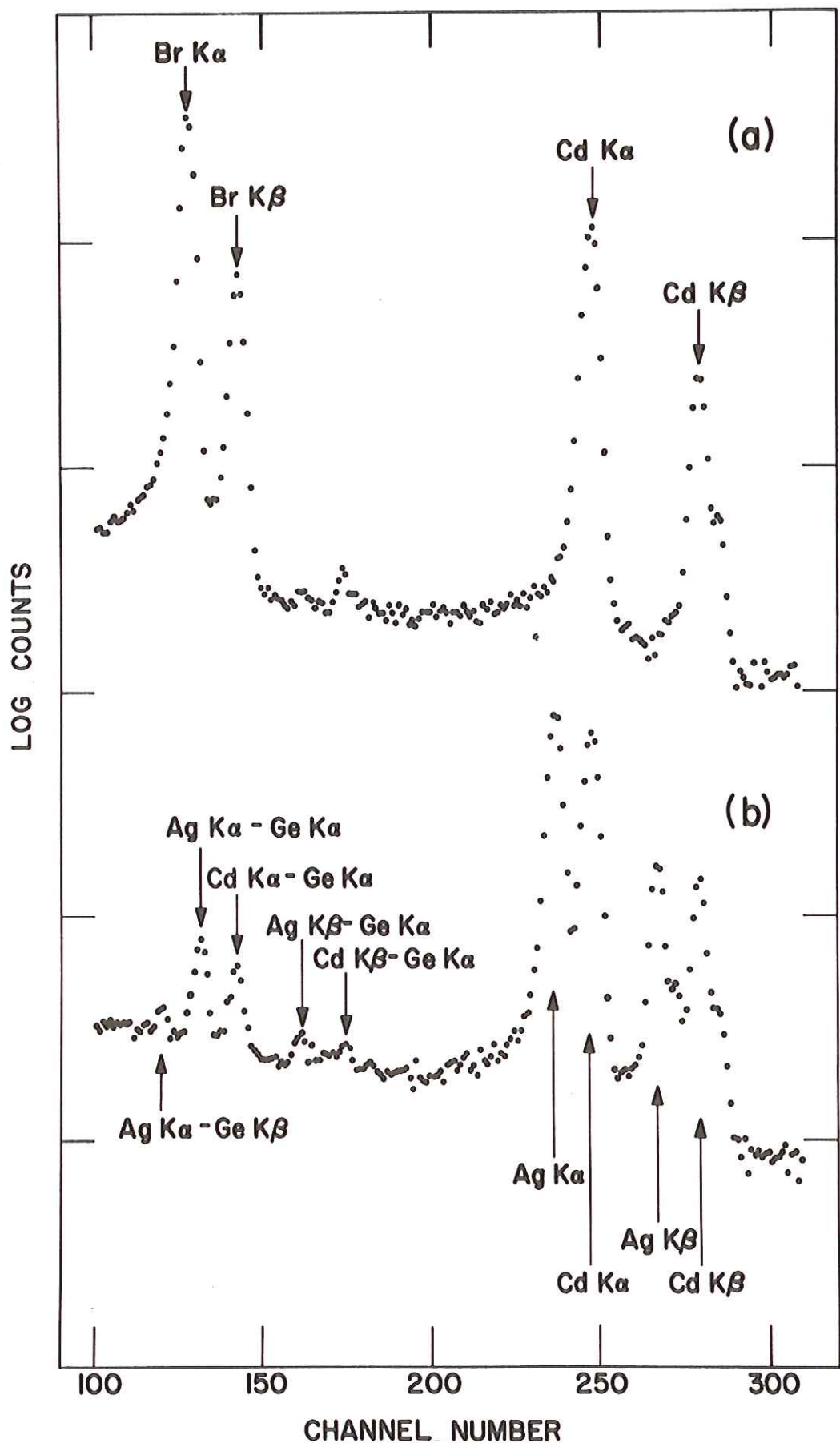


FIGURE 3.3

Typical X-Ray Spectra of the Reference Samples
Obtained with the Ge(Li) Detector (System C)

- (a) Br/Cd (atom ratio: 2) after 5 minute run with 2 MeV electron at 30 nA current.
- (b) Ag/Cd (atom ratio: 0.9754) after 2 minute run with 2 MeV electrons at 45 nA current.



efficient a detector as Ge(Li). Therefore, the Si(Li) detector is in general a more useful detector for elemental analysis.

The relative yields must be accurately known to be useful for quantitative elemental analysis or for obtaining the ionization cross sections (Section 3.2). Beside the random uncertainties in the values of the atom ratios and the measured X-ray intensities, there are a number of factors which could introduce systematic errors into the relative yields. These factors are related to the constancy of the atom ratio throughout the target preparation and measurement, and the differences in the X-ray production and detection due to target matrix effects.

The uncertainties in the atom ratios due to random errors in weighing the sample reagents are trivial. At most, they are only several tenths of one percent. The two assumptions, a) that the sample reagents are chemically pure and b) that the atom ratio in a sample solution is exactly equal to the ratio in the target, are much more serious and could introduce a considerable systematic error. These two assumptions were considered and discussed in Sections 2.2.2 and 2.2.3, respectively. The uncertainty due to the unknown chemical purity of the reagents is estimated to be 1-2%. The second assumption (b) was found in the two test cases studied to be valid within their measurement precision (see Tables 2.8 and 2.9). Except with very small atom ratios, this precision is of the order of 1-5%. Another possible contribution to systematic error which has the effect of changing the atom ratio is the decomposition of the target during the measurement. Electron irradiation may cause sample decomposition by vaporization, polymerization,

recrystallization, desorption of absorbed gas, etc. The various processes are not well understood [cf. Kircher and Bowman (KB64)], but the possibility of sample change during the electron bombardment should not be overlooked. Any process which preferentially depletes one element from the target during the measurement will drastically alter the effective atom ratio. This was, in fact, evidenced with targets containing bromides, e.g. the Hg/Br filter paper reference target. It was found that bromine was lost in comparison to the other element, e.g. Hg, during the irradiation and measurement. For this reason, the original choice of bromine as the primary reference element was supplanted with cadmium (see Section 2.2.2). This effect was not observed for any other element used in the targets.

The errors in the relative yields due to the statistical uncertainty in the X-ray intensities are minimal in most cases. The major contribution to this uncertainty is in locating the "true" background under the X-ray peaks (see Equation 2.1). This uncertainty is less than 1% (approximately 10^4 net counts) for all the K α X-ray yields. The only cases for which it is greater than $\sim 3\%$ (i.e., 10^3 net counts) are for some of the K β X-ray yields where the detection efficiency for the corresponding K β X-rays was low.

The differences in the measured X-ray intensities due to target matrix effects can introduce systematic errors into the relative yields, and in turn affect the accuracy for quantitative elemental analysis. These effects have been considered in detail by many workers [cf. Birks (B69), Gould and Bates (GB72) and Müller (M72)]. In brief, these effects arise from the enhancement of the X-ray intensity due to

excitation by bremsstrahlung produced in the target and by the secondary fluorescence of one element by the X-rays from another element, and from the attenuation of the X-ray intensity by self-absorption in the target. These effects can be quite large [cf. Müller (M72), p. 70] depending on the specific constituency of the sample target. With the lens tissue targets used in these studies, the matrix effects are unimportant. This is mainly due to the fact that these targets contain less than 1 mg/cm² of any element (see Section 2.2). For a target with two elements, A and B, the magnitude of secondary fluorescence of element B by the X-rays of element A depends upon the relative amounts of the two elements and the energy separation of the X-ray of element A and the absorption edge of element B. Even assuming that the X-ray energy for A is perfectly matched with the absorption edge for B, the ratio of element B X-rays from secondary fluorescence and from direct electron impact ionization is much less than 1% for the lens tissue targets with a a_A/a_B atom ratio of unity.

Li-Scholz, et. al. (LSS72) have conclusively demonstrated that the enhancement of the X-ray intensity due to bremsstrahlung produced in the target is only of the order of 1% for any of the elements in these lens tissue targets. The ratio of the number of bremsstrahlung-produced K-shell holes per electron* to the number of K-shell holes produced by

*The bremsstrahlung contribution was estimated using the differential radiative cross section for bremsstrahlung [cf. Evans (E55), p. 603] to obtain the number of bremsstrahlung quanta in a given energy interval per electron. The photoelectric absorption of these quanta was then used to calculate the number of K-shell holes per electron.

direct electron excitation[†] was calculated for a variety of three component targets containing elements C (representing paper), Cd and Z. They considered the ionization of each element by the bremsstrahlung due to itself or to the other two elements. The bremsstrahlung contribution to the X-ray intensity of either element Z or Cd was found to be only 0.7% to 1.2% for all the Z/Cd targets in the range from Z = 24 to Z = 82. Again, it must be emphatically stated that this was only due to the thinness of the lens tissue targets. It would not be applicable to the filter paper targets which are over five times thicker.

The last matrix effect to be considered is that of self-absorption of the X-rays in the targets. As before, this effect also depends on the amounts and the constituents making up the targets. It, in addition, is largest for low energy X-rays which are more strongly absorbed. The transmission of K α X-rays from the lens tissue reference targets was measured for eighteen different Z/Cd targets, ranging from Z = 23 to Z = 51. These measurements are described in Appendix B. The self-absorption in the lens tissue targets was negligible for elements greater than Z ~ 40, while the absorption was nearly 20% at Z ~ 25. Furthermore, due to the similarity of the target preparations, the transmission of K α X-rays of element Z was found to vary regularly with the atomic number, Z. Similar measurements (see Appendix B) were made to determine the self-absorption of the Cu K α X-rays in the NBS metal alloy sample targets. The differences in the absorption in the Cu/Cd

[†]The direct electron excitation contribution was calculated using the theory of Kolbenstvedt (K67) (see Section 1.1.2).

reference target and in the NBS sample targets was found to be \sim 5%. The agreement with the NBS sample targets containing Cd was better (\sim 2%). This was to be expected. Since these latter targets containing Cd would more closely resemble the reference targets. At any rate, the self-absorption differences in the reference targets and unknown targets are compensated to first order.

The precision of the relative yields appears to be of the order of several percent. The $Y_{K\beta}(Cd)$ yields measured for each target in the three systems is provided in Tables 3.1 through 3.3. Since these values do not depend on the atom ratios, they are indicative of the precision of the spectrum analysis procedure (i.e., obtaining the measured X-ray intensities). In general, the values are within 2% of the average for a given system. In comparison, the yields $Y_{K\alpha}(Br)$ and $Y_{K\beta}(Br)$ for bromine obtained with System B (Table 3.1) are not in as good agreement. These yields depend not only on the accuracy of the spectrum analysis, but also on the accuracy of the atom ratios. It is not conclusive whether they reflect the true precision of the relative yields since there is the uncertainty in the stability of the targets containing bromine. A more accurate indicator of the precision is to obtain the yields from measurements of the same target prepared twice. This was done in System D for the two targets Nd/Cd and Gd/Cd. Both sets of measured values are provided in Table 3.3. As shown, the $Y_{K\alpha}(Z)$ yield agree to \sim 1%. The reproducibility of the $K\beta$ X-ray yields, $Y_{K\beta}(Z)$, for the two cases is not as good. This is mainly a result of the uncertainty in the measured $K\beta$ X-ray peak intensities. The major contribution to this uncertainty is not statistical, but rather the inherent

error in locating the "true" background under the peak. In these cases, where the peaks are not very large due to the low detection efficiency, the net peak intensities are very sensitive to the background subtraction. Lastly, a critical test of the precision was made by measuring the ratio of V K α X-rays to Zn K α X-rays in a V/Zn target (see Table 2.2). This value was compared to the Y_{K α} (V)/Y_{K α} (Zn) ratio obtained from the V/Cd and Zn/Cd targets. The two results agreed to 3%.

In consideration of all of these factors, including matrix effects, the error limits of the relative yields are estimated to be $\pm 5\%$. The only cases for which this accuracy is not anticipated are the yields of the light elements ($Z < 20$) in System D and the K β X-ray yields, Y_{K β} (Z), of the heavy elements ($Z > 60$) in all three systems.

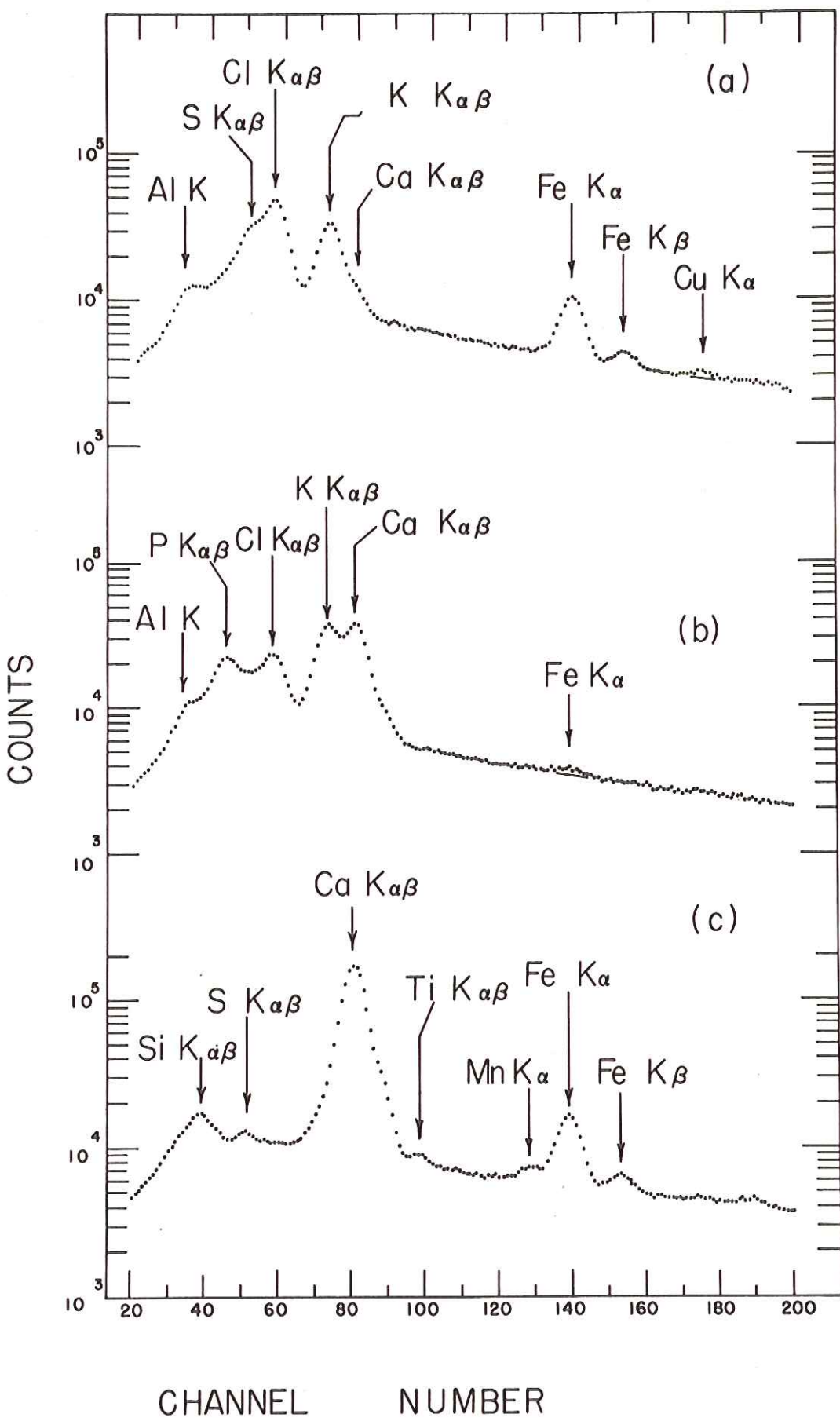
Qualitative elemental analysis is straight forward. All that is necessary is the proper identification of the X-ray peaks in the spectrum. The method is well suited for the analysis of completely unknown samples since the detectable K and L X-rays of all the elements contained in the sample are obtained simultaneously. In this regard, it should be noted that a preliminary qualitative measurement on an unknown sample can be made to rapidly ascertain the major constituents of the sample. This knowledge can be an aid in choosing the best procedure for quantitative measurements, or for selecting the most suitable solvent for dissolving the solid unknown.

For demonstrative purposes, three spectra are shown in Figure 3.4 as examples of qualitative analysis of completely unknown samples. The first spectrum (Figure 3.4a) is that obtained from human

FIGURE 3.4

Typical Low Energy X-Ray Spectra Obtained with
the Si(Li) Detector (System D)

- (a) Whole blood (man) adsorped onto a lens tissue target after 229 minute run at 40 nA current.
- (b) Milk (dairy cow) adsorped onto a lens tissue target after 67 minute run at 70 nA current.
- (c) Leaf (oak) after 128 minute run at 35 nA current.



blood. The target was prepared by adsorbing a small amount (< 1 ml) of whole blood onto a lens tissue. The second spectrum (Figure 3.4b) is that obtained from commercial dairy cow milk adsorbed onto the lens tissue. The final spectrum (Figure 3.4c) is that from an oak tree leaf which served as its own supporting matrix. These examples also demonstrate the use of both liquid and solid samples without further treatment. Each of the three spectra clearly indicate the presence of at least six elements in the low energy region shown. The X-ray lines are not resolved very well in this region, but they are suitable for qualitative analysis. For example, the relative X-ray intensities for the elements S, Cl, K, Ca and Fe in the blood spectrum (Figure 3.4a) are in good correspondence with known concentrations of these elements in the blood of man.* In the present system, the lightest detectable element was aluminum. This limit was attained only because the Si(Li) detector was vacuum coupled to the target chamber. It was not possible in the other systems which employed air paths because the absorption of low energy X-rays was too strong.

To demonstrate and evaluate the method for quantitative elemental analysis, three NBS metal alloy samples were assayed. Each of the three alloys consists of 6-7 metals ranging in concentration from 88% to 0.1%. Thus, they should be useful in testing the method's capability for detection and determination of both major and minor constituents over a wide range of elements. The samples were assayed

*Concentrations (in ppm) of the elements in the blood of man: P, 145; S, 1220; Cl, 4500; K, 157; Ca, 102; Fe, 1.0; Cu, 1.3; Zn, 1.1; Br, 5.0; Cd, 1.0; see Gofman, et. al. (G62).

using System C and D. For the assays, analysis of the K X-rays were used exclusively, except with the Si(Li) detector (System D) in the case of the Pb determination where the L X-rays were used. The Ge(Li) detector (System C) was used only for determination of elements above tin.

The results for the determination of the m_{Sb}/m_{Sn} and m_{Pb}/m_{Sn} weight ratios in the three NBS samples are provided in Table 3.4. Typical spectra of one of the NBS samples used for these measurements are shown in Figure 3.5 for the phosphor bronze bearing metal (NBS No. 63). With the Ge(Li) detector, both Sb and Pb were determined relative to Sn by measurements of the K α X-ray intensities of the three elements in the same spectrum. The determinations with the Si(Li) detector were made using the Sn K α and Sb K α X-rays for the m_{Sn}/m_{Sb} weight ratio, and the Sn K α and the Pb L α_1 or L β X-ray lines for the m_{Pb}/m_{Sn} weight ratio. The relative yields for the two Pb L lines were obtained from the Pb/Cd reference sample (see Figure 3.2c) in a similar manner to that used to obtain the relative K X-ray yields. They are, relative to the Cd K α , 4.221 for the Pb L α_1 and 2.928 for the Pb L β . As seen in Table 3.4, the results for the m_{Pb}/m_{Sn} analyses with the Si(Li) detector are in general in better agreement with the reported values than those obtained with the Ge(Li) detector. The more accurate results with the Si(Li) detector may be due to better counting statistics. The relative yield for the Pb L α_1 with the Si(Li) detector is almost 20 times larger than the Pb K α yield with the Ge(Li) detector. Therefore, to achieve the same counting statistics for this case, the Ge(Li) run would need a 20 times longer counting time at the same electron current. Furthermore,